JOURNAL OF SOLID STATE CHEMISTRY 107, 194–200 (1993)

Preparation and Physical Properties of the Delafossite-Type Solid Solutions $AgCo_xNi_{1-x}O_2 (0 \leq x \leq 0.5)$

Y. J. SHIN, J. P. DOUMERC,* P. DORDOR, M. POUCHARD, AND P. HAGENMULLER

Laboratoire de Chimie du Solide du CNRS, 351, Cours de la Libération, 33405 Talence Cedex, France

Received October 19, 1992; in revised form February 15, 1993; accepted February 17, 1993

Delafossite-type $AgCo_xNi_{1-x}O_2 (0 \leq x \leq 0.5)$ solid solutions have been prepared by an exchange reaction of the corresponding Na compounds with molten $AgNO_3$. Magnetic and electrical properties have been investigated. The metal–insulator transition observed as x increases has been ascribed to a vanishing of the 4*d* (Ag)–σ^*(Ni–O) band overlapping previously invoked for describing $AgNiO_2$ as a semimetal. © 1993 Academic Press, Inc.

1. Introduction

The electrical transport properties of delafossite compounds $A^IM^{III}O_2$ mainly depend on the nature of the A^+ cation. For A^+ cations with a d^{10} configuration such as Cu^+ and Ag^+ delafossite-type oxides are insulators whereas $PdCrO_2$, $PdCoO_2$, and $PtCoO_2$ are metallic. This behavior was simply explained by the Rogers band diagram (*1*). However, we have recently reported that despite the fact that A^+ is a silver (*I*) cation $AgNiO_2$ exhibits a metallic type conduction which we have attributed to a small overlapping between the 4*d* (Ag) and the σ^*(Ni–O) bands (*2*, *3*). Such a band overlap does not occur in $AgCoO_2$ since it is an insulator like all other delafossite-type Cu^+- or Ag^+-compounds.

This strong difference in the electrical transport properties between $AgNiO_2$ and $AgCoO_2$ led us to investigate the solid solution $AgCo_xNi_{1-x}O_2$.

* To whom correspondence should be addressed.

2. Experimental Conditions

Delafossite Ag-compounds are usually prepared by cation exchange reactions in oxidizing ($AgNO_3$ + KNO_3) fluxes using alkali metalates with α-$NaFeO_2$ structure such as $LiMO_2$ or $NaMO_2$, as intermediate compounds (*4*, *5*). As such exchange reactions are performed at moderate temperatures ($T < 300$°C), the structural disorder or defects present in the intermediate compounds influence those observed in the resulting delafossite phases as we have shown recently (*3*). As $LiNiO_2$ exhibits a slight nonstoichiometry and a small disorder between Li and Ni atoms (*6*, *7*), we have chosen Na oxides as intermediate compounds. They are prepared by solid state reaction in an oxygen atmosphere at 650°C, following the reactional scheme:

$$\tfrac{1}{2}\,Na_2O_2 + x/3Co_3O_4 + (1-x)NiO \rightarrow NaCo_xNi_{1-x}O_2$$

The reaction product contains a single phase only for $0 \leq x \leq 0.5$. For $x > 0.5$, it contains two phases: $NaCoO_2$ and $NaCo_{0.5}Ni_{0.5}O_2$,

0022-4596/93 $5.00

as observed earlier (*8*). Therefore, the exchange reactions

$$AgNO_{3(l)} + NaCo_xNi_{1-x}O_{2(s)} \xrightarrow{KNO_3} AgCo_xNi_{1-x}O_{2(s)} + NaNO_{3(l)}$$

were performed for $0 \leq x \leq 0.5$ and $x = 1$. KNO_3 was added to prevent the decomposition of $AgNO_3$ and an excess of $AgNO_3$ (~50%) was used to promote the reaction. Reactions were carried out in evacuated and sealed pyrex tubes at 300°C for 5 days. Grey black powders were recovered by leaching out the remaining nitrates with water.

Powder X-ray diffractograms were obtained with a Philips 1050 diffractometer using a copper anticathode. Lattice constants were determined by a least squares method from the *d*-values and corrected using silicon as an internal standard ($a = 5.4305$ Å at 25°C).

Magnetic susceptibility was measured with a Manics DSM 8 type susceptometer.

Electrical conductivity measurements were performed on pellets ($\phi = 5$ mm density ≈70%) using a usual four-probe technique (*9*). Thermoelectric power was measured by means of a piece of equipment described elsewhere (*10*).

3. Results and Discussion

3.1. X-Ray Diffraction

$AgCo_xNi_{1-x}O_2$ compounds ($0 \leq x \leq 0.5$; $x = 1$) crystallize with the $3R$-delafossite structure (space group $R\bar{3}m$). In this structure monovalent cations are linearly coordinated to two oxygen atoms forming AO_2^{3-} groups parallel to the hexagonal *c*-axis. These groups form a close packing where octahedral sites are occupied by the M^{3+} cations (Fig. 1).

Whatever the x value, X-ray diffractograms do not reveal any extra line that could have resulted from the existence of an ordering between Co and Ni atoms. The unit cell volume increases as x decreases (Fig. 2); this simply can be attributed to a smaller ionic radius (*11*) for Co^{3+} ($r_{Co^{3+}} = 0.545$ Å) than for Ni^{3+} ($r_{Ni^{3+}} = 0.56$ Å). However, this volume increase does not result from an isotropic expansion of the unit cell since, as shown in Fig. 3, the *a*-parameter decreases significantly with the Co-content whereas the *c*-parameter remains nearly independent of x. Such a behavior is usual for delafossite compounds as pointed out previously (*4*): it results from an increase of the trigonal distortion of the MO_6 octahedra as the ionic radius of the *M*-element increases. We may think that the linear coordination of the A^+

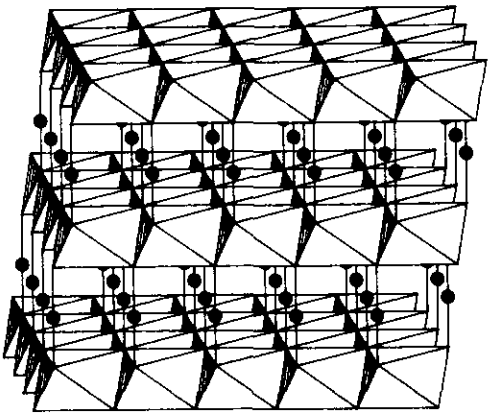

FIG. 1. Delafossite-type structure of AMO_2 oxides. Circles represent A^+ ions located between layers of MO_6 octahedra.

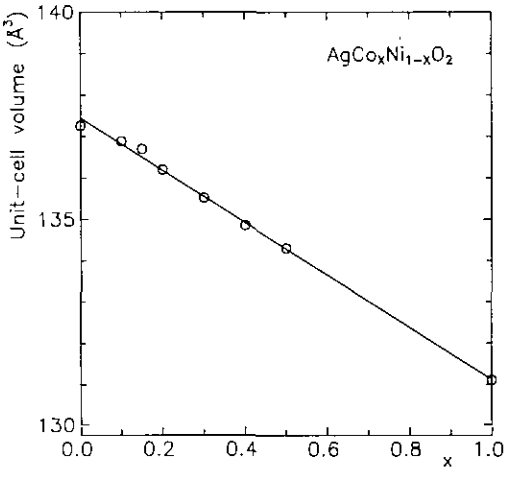

FIG. 2. Evolution with x of the hexagonal unit cell volume of the $AgCo_xNi_{1-x}O_2$ solid solutions.

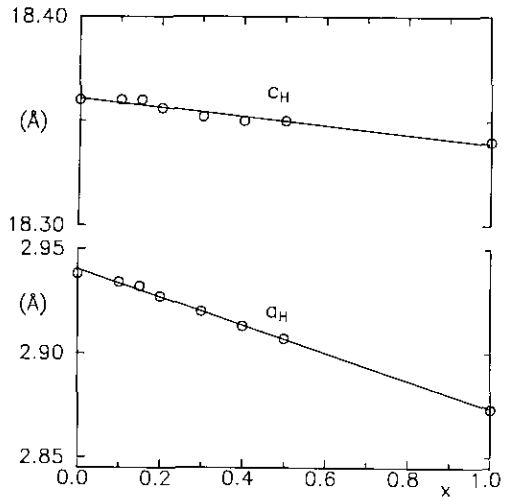

FIG. 3. Evolution with x of the hexagonal lattice constants a_H and c_H of the $AgCo_xNi_{1-x}O_2$ solid solutions.

ions in delafossite compounds allows large changes in the ionic radii of M^{3+} cations (from $r^{VI}_{Al^{3+}} = 0.535$ Å to $r^{VI}_{La^{3+}} = 1.032$ Å) as far this trigonal distortion does not modify the A-site. On the contrary, the α-$NaFeO_2$ structure, in which the A-cation occupies an octahedral site, does not seem to be stable for an r_A/r_M ratio smaller than 1.1 or larger than 2.0 (*12*).

3.2. *Magnetic Properties*

The thermal variation of reciprocal magnetic susceptibility of $AgCo_xNi_{1-x}O_2$ (x = 0, 0.1, 0.2, 0.5, 1) is given in Fig. 4. The experimental data corrected for the diamagnetism of the ions (*13*) were fitted above a temperature T_m (given in Table I) with the usual Curie–Weiss formula, $\chi_M = c_M/(T - \theta_p)$ + TIP. The molar Curie constant C_M, the Weiss constant θ_p, and the temperature-independent paramagnetic contribution TIP are reported in Table I. For $0 \leq x \leq 0.5$, the Curie constant for one Ni atom is in the range of 0.40–0.46, which suggests that both Ni^{3+} and Co^{3+} ions exhibit mainly a low-spin configuration, i.e., atomic ground terms ^2E (t^6e^1; $S = \frac{1}{2}$) and ^1A (t^6e^0; $S = 0$) respectively. It also implies that no significant

$$Ni^{3+} + Co^{3+} \rightarrow Ni^{2+} + Co^{4+} \quad (1)$$
$$S = \tfrac{1}{2} \quad S = 0 \quad S = 1 \quad S = \tfrac{1}{2}$$

charge transfer occurs. For a $Ni^{3+} + Co^{3+} \rightarrow Ni^{4+} + Co^{2+}$ charge transfer to agree with our magnetic data would require that Ni^{4+} and even Co^{2+} had a low-spin configuration, which is quite unlikely in our compounds for the latter cation. On the other hand, we may assume that such a charge transfer does not occur because Ni^{3+} ions are more oxidizing than Co^{3+} ions as recently shown, for instances, for α-$NaFeO_2$ type compounds (*14*).

The negative values of θ_p reveal the existence of antiferromagnetic interactions between Ni-ions giving rise to a minimum in the χ_M^{-1} vs T plots for $x \leq 0.1$. As x increases $|J|$ should increase since the Ni–Ni distance which is equal to the a-parameter decreases. Therefore, the observed decrease of $|\theta_p|$ is mainly due to the decrease of the number of magnetic nearest neighbors as the Ni-concentration is more and more diluted. For $x \geq 0.2$, the minimum of χ_M^{-1} disappears and at low temperature χ_M increases with x despite smaller and smaller Ni^{3+}-concentration (Fig. 4).

The weak paramagnetism of $AgCoO_2$ confirms the low-spin state of Co^{3+} (^1A term).

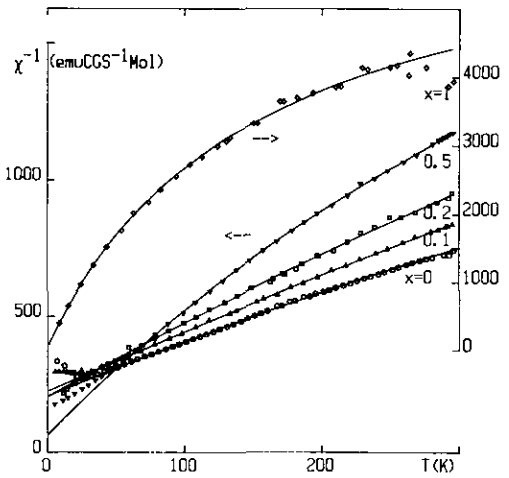

FIG. 4. Thermal variation of the reciprocal molar magnetic susceptibility of $AgCo_xNi_{1-x}O_2$.

TABLE I

EXPERIMENTAL MAGNETIC PARAMETERS OF Ag–DELAFOSSITE COMPOUNDS $AgCo_xNi_{1-x}O_2$.

Samples	T_m(K)	C_M (emu K mole^{-1})	C_M/Ni-mole (emu K mole^{-1})	θ_p(K)	TIP (10^{-6} emu mole^{-1})
$AgNiO_2$	24.5	0.46	0.46	−105	200
$AgCo_{0.1}Ni_{0.9}O_2$	19	0.42	0.46	−99	106
$AgCo_{0.2}Ni_{0.8}O_2$	—	0.33	0.41	−69	150
$AgCo_{0.5}Ni_{0.5}O_2$	—	0.20	0.40	−13	200
$AgCoO_2$	—	0.02	—	0	150

The temperature-dependent contribution might be attributed either to a small amount of HS Co^{3+} associated with structural defects or surface states. We may also consider Co^{2+} or Co^{4+} impurities due to vacancies of either oxygen or metallic atoms respectively. The concentration of such impurities is difficult to determine, but in the case of HS Co^{2+}, for instance, it may be roughly estimated as being of the order of 1 mole% using a spin-only Curie constant $C_M^{SO} = 1.875$. The temperature independent contribution is also of the order of magnitude normally expected for an A term (*15*).

3.3. Electrical Properties

Figure 5 gives the variation of the thermoelectric power α of some $AgCo_xNi_{1-x}O_2$ solid solutions ($0 \leq x \leq 0.4$) as a function of temperature. For $0 \leq x \leq 0.3$, α is positive at low temperature, increases with temperature, exhibits a maximum α_{max} at a temperature T_{max} and finally changes its sign at a temperature T_S^α. At rising x, α_{max}, T_{max}^α and T_S^α decrease. For $x = 0.4$ α is negative in the whole temperature range and its absolute value increases with T. For pure $AgCoO_2$ ($x = 1$) a large positive value ($\alpha \simeq +150$ μV K^{-1}) is observed revealing that the charge carriers are mainly holes.[1]

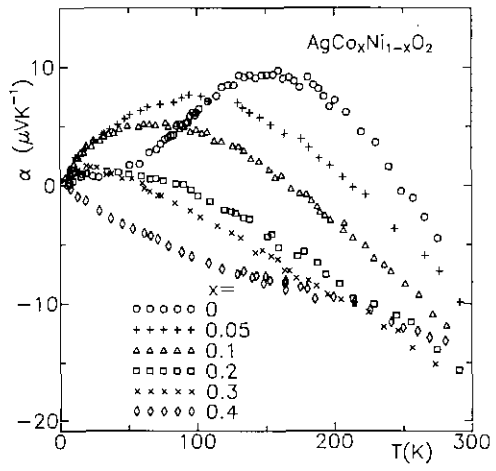

FIG. 5. Thermal variation of the thermoelectric power of $AgCo_xNi_{1-x}O_2$.

The logarithm of the electrical resistivity ρ is plotted vs T in Fig. 6a for $0 \leq x \leq 0.5$ and for $x = 1$. As x increases the low temperature behavior changes from a metallic one for $x \leq 0.2$ as $\rho(T \to 0\ K)$ tends to a finite value to an insulating one for $x \geq 0.3$ as $\rho(T \to 0\ K) \to \infty$. As expected a metal–insulator transition is observed for $x \simeq 0.3$ and above this value the electrical conductivity is thermally activated in the whole temperature range (Fig. 6).

The behavior of $AgNiO_2$ ($x = 0$) has been already discussed on the basis of a semimetal model (*2*, *3*). As mentioned above, charge carriers are created by a small overlap of the 4*d* (Ag) band with the σ^*(Ni–O) band, which can be illustrated by the chemical equilibrium:

$$Ag^+ + Ni^{3+} \rightleftarrows \text{“}Ag^{2+}\text{”} + Ni^{2+}.$$

[1] This supports the opinion that the magnetic behavior is rather due to LS Co^{4+} species resulting likely from a slight silver or cobalt deficiency.

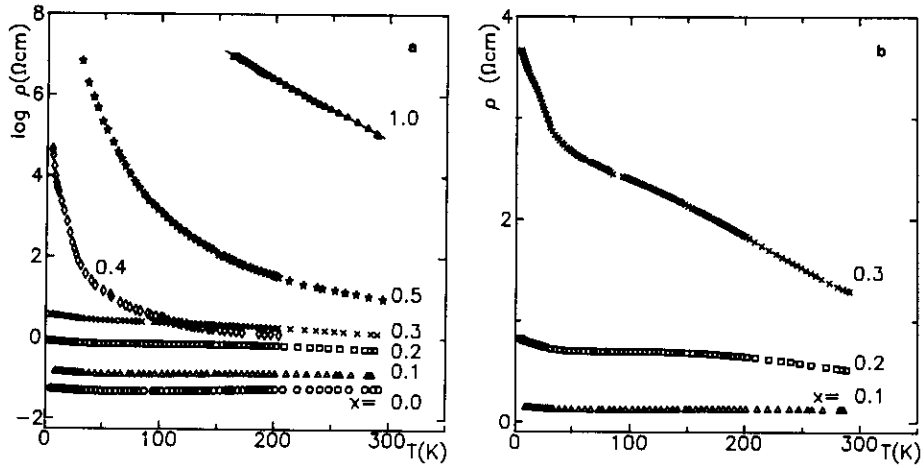

FIG. 6. Thermal variation of the electrical resistivity of $AgCo_xNi_{1-x}O_2$ plotted for $0 \leq x \leq 0.5$ and $x = 1$ using either semilogarithmic coordinates (a) or natural ones for $0.1 \leq x \leq 0.3$ (b).

Assuming that, as argued above, most nickel and cobalt ions are in the 3+ oxidation state, three main effects are expected to occur as the Ni^{3+} concentration decreases:

(a) as shown in Fig. 2 the a-parameter decreases, which is mainly due to a decrease of the M^{3+}–O distances. This should lead to an increase of the Ni–O bond covalency and hence to a shift of the antibonding σ^*(Ni–O) level toward higher energies.

(b) A narrowing of the σ^*(Ni–O) band if we assume that the dilution effect overcomes the covalency increase.

(c) Some structural disorder due to a random distribution of Ni^{3+} and Co^{3+} cations. It can lead to the formation of band tails where energy levels can be localized depending on their energy with respect to a mobility edge E_c (*16*).

The (a) and (b) effects lead to a decrease of the 4*d* (Ag)–σ^*(Ni–O) band overlapping responsible for the semimetallic character of $AgNiO_2$ and therefore simply account for the evolution of the electrical resistivity with x and finally for the metal–insulator transition observed for $x \simeq 0.3$.

However, the thermal variation of the thermoelectric power does not reveal, even for $x = 0.4$, the existence of an energy gap as it should be expected from the above model, but it suggests a finite density of states at the Fermi level.

As x increases the temperature at which α changes its sign, i.e., T_S^{α}, decreases. If both electrons and holes can carry current, the usual formula

$$\alpha = \frac{\alpha_e \sigma_e + \alpha_h \sigma_h}{\sigma_e + \sigma_h}$$

applies, where the subscripts e and h refer to electrons and holes respectively. Therefore, as x increases, the temperature above which the contribution of electrons to the electrical conductivity becomes predominant decreases. We may think that although the shrinking of the Ni–Ni distance (equal to the a-parameter) as x increases should make the electron hopping easier, the competing dilution effect prevails, and finally diminishes the hopping probability. Therefore, the tendency of α to become negative in a wider temperature range suggests that the electron density, rather than the mobility, increases due to either extrinsic or intrinsic effect. In the first hypothesis, an extrinsic creation of electrons would simply result from a slight oxygen nonstoichiometry or a deficiency of AgO_2^{3-} groups and the Co^{3+}/Ni^{3+} substitution would favor these vacancies for unknown reasons. In the second

hypothesis, the present results and particularly the α vs T behavior suggest that a small number of electrons are transferred from the t_{2g} orbitals of Co^{3+} into the e_g orbitals of Ni^{3+} according to equilibrium (1). Magnetic measurements have excluded the formation of large amounts of Ni^{2+} and Co^{4+} but have not excluded a tiny electronic transfer. Such a small amount of Co^{4+} and Ni^{2+} could be stabilized by structural disorder which can give rise to some local potential fluctuations appropriate to trap holes on cobalt sites whereas a few electrons would be located on nickel sites where they can hop from one position to another. In conclusion, as x increases the electron-density/Ni-density ratio increases, explaining the evolution of the α vs T curves, but the electron mobility decreases as the hopping probability decreases with reduced nickel concentration, which accounts for the evolution of the ρ vs T curves.

In the above approach the metal–insulator transition roughly occurs when the hole concentration tends to zero; i.e., when the band overlap disappears, or just before, when the Fermi level crosses the mobility edge near the top of the 4*d* (Ag) band, which could explain that even for $x = 0.3$, α remains slightly positive at low temperature while this composition is probably on the insulating side of the transition, as suggested by the ρ vs T curves of Fig. 6b.

3.4. *Energy Correlation Diagram*

In the framework of a purely ionic model, we may use our calculations of site potential in $AgNiO_2$ (*3*) in order to estimate the electron potential energy at the various ion sites in the $AgCo_xNi_{1-x}O_2$ lattice, according to the simple equation

$$E = -IE^N - eV_M, \qquad (2)$$

where IE^N is the Nth ionization energy, V_M the Madelung electrostatic potential, and $-e$ the electron charge.

The data of Table II lead to the schematic diagram of the left hand side of Fig. 7. The evolution with x of the band diagram shown in the right hand side of Fig. 7 can be deduced from the results reported and discussed in the above sections and from previous investigations on $AgCoO_2$ and $AgNiO_2$ (*3*). For $0 \leq x < 0.3$, the 4*d* (Ag) levels overlap the UHB(Ni). As equilibrium (1) is strongly shifted to the left hand side the t_{2g}(Co) levels are below the UHB of nickel although a small overlapping well accounts for the behavior of thermoelectric power as suggested above.

TABLE II

POTENTIAL ENERGY OF ELECTRONS AT VARIOUS ION-SITES IN $AgCo_xNi_{1-x}O_2$ ESTIMATED FROM EQ. (2)

Ion-site	IE^N (eV)[a]	V_M (V)[b]	E (eV)
$Ag^{+/2+}$	21.5	−9.5	−12
$Co^{3+/4+}$	51.3	−37.1	−14.2
$Ni^{3+/4+}$	54.9	−37.1	−17.8
$O^{2-/-}$	−8.1	24.2	−16.1

[a] From Ref. (*17*).
[b] From Ref. (*3*).

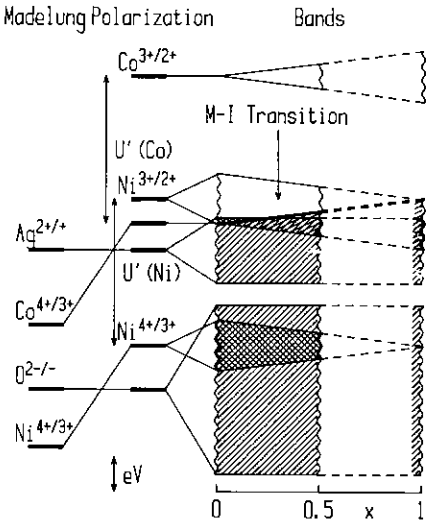

FIG. 7. Tentative correlation diagram between (from left to right) energy levels of ions in the Madelung potential (without and with polarization effects) and energy bands for $AgCo_xNi_{1-x}O_2$ ($0 \leq x \leq 0.5$) and $AgCoO_2$ (see text).

The correlation between the ionic energy levels in the Madelung potential and the band diagram involves polarization effects which raise occupied levels (*18*). To simplify, we have taken the oxygen levels as reference levels and assumed a shift of the Ag^+ levels under polarization effects close to that of the $O^{2-/-}$ levels. A polarization shift smaller for $Ag^{+/2+}$ levels than for $Ni^{3+/4+}$ or $Co^{3+/4+}$ levels could result from the twofold coordination of Ag^+ with respect to the octahedral environment of Ni^{3+} or Co^{3+} ions.

In conclusion, this picture shows that assuming a reasonable value of U' for $Ni^{3+/4+}$–$Ni^{2+/3+}$, i.e., ~4 eV, makes quite possible the suggested overlapping between the Co^{3+} : t_{2g} levels and the UHB of nickel. It also accounts for the already proposed $4d(Ag)$–$\sigma^*(Ni–O)$ band overlap as well as for the insulating character of $AgCoO_2$.

Acknowledgments

The authors thank C. Delmas and I. Saadoune for helpful discussions. They are also indebted to J. C. Grenier for valuable advice and help in magnetic measurements and to E. Marquestaut for electrical measurements. One of them (Y. J. Shin) is grateful for the financial support of Sunkyong Magnetics, Ltd. (Seoul, ROK).

References

1. D. B. Rogers, R. D. Shannon, C. T. Prewitt, and J. L. Gillson. *Inorg. Chem.* **10,** 723 (1971).
2. A. Wichainchai, P. Dordor, J. P. Doumerc, E. Marquestaut, M. Pouchard, and P. Hagenmuller, *J. Solid State Chem.* **74,** 126 (1988).
3. Y. J. Shin, J. P. Doumerc, P. Dorder, C. Delmas, M. Pouchard, and P. Hagenmuller, submitted for publication.
4. J. P. Doumerc, A. Ammar, A. Wichainchai, M. Pouchard, and P. Hagenmuller, *J. Phys. Chem. Solids* **48,** 37 (1987).
5. R. D. Shannon, D. B. Rogers, and C. T. Prewitt, *Inorg. Chem.* **10,** 713 (1971).
6. G. Dutta, A. Manthiram, J. B. Goodenough, and J.-C. Grenier, *J. Solid State Chem.* **96,** 123 (1992).
7. I. Saadoune, Thesis, University of Bordeaux I (1992).
8. C. Delmas, Y. Borthomieu, C. Faure, A. Delahaye, and M. Figlarz, *Solid State Ionics* **32/33,** 104 (1989).
9. P. Dordor, E. Marquestaut, C. Salducci, and P. Hagenmuller, *Rev. Phys. Appl.* **20,** 795 (1985).
10. P. Dorder, E. Marquestaut, and G. Villeneuve, *Rev. Phys. Appl.* **15,** 1607 (1980).
11. R. D. Shannon, *Acta Crystallogr. Sect. A* **32,** 751 (1976).
12. M. Brunel, F. de Bergevin, and M. Gondraud, *J. Phys. Chem. Solids* **33,** 1927 (1972).
13. Landolt-Börnstein, Vol. II, Springer-Verlag, Berlin-Heidelberg-New York (1966).
14. C. Delmas, private communication (1992).
15. B. N. Figgis, "Introduction to Ligand Fields," Interscience, New York-London-Sydney (1961).
16. N. F. Mott, "Metal–Insulator Transitions," 2nd ed., Taylor & Francis Press, London-New York-Philadelphia (1991).
17. J. E. Huheey, "Inorganic Chemistry," 2nd Ed., Harper and Row, New York (1978).
18. P. A. Cox, "The Electronic Structure and Chemistry of Solids," Oxford Univ. Press, Oxford-New York-Tokyo (1987).